

Accepted Manuscript

Synthesis of (Z)-1-(1,3-diphenyl-1H-pyrazol-4-yl)-3-(phenylamino)prop-2-en-1-one derivatives as potential anticancer and apoptosis inducing agents

T. Srinivasa Reddy, V. Ganga Reddy, Hitesh Kulhari, Ravi Shukla, Ahmed Kamal, Vipul Bansal



PII: S0223-5234(16)30233-1

DOI: [10.1016/j.ejmech.2016.03.051](https://doi.org/10.1016/j.ejmech.2016.03.051)

Reference: EJMECH 8476

To appear in: *European Journal of Medicinal Chemistry*

Received Date: 31 January 2016

Revised Date: 17 March 2016

Accepted Date: 18 March 2016

Please cite this article as: T. Srinivasa Reddy, V. Ganga Reddy, H. Kulhari, R. Shukla, A. Kamal, V. Bansal, Synthesis of (Z)-1-(1,3-diphenyl-1H-pyrazol-4-yl)-3-(phenylamino)prop-2-en-1-one derivatives as potential anticancer and apoptosis inducing agents, *European Journal of Medicinal Chemistry* (2016), doi: 10.1016/j.ejmech.2016.03.051.

This is a PDF file of an unedited manuscript that has been accepted for publication. As a service to our customers we are providing this early version of the manuscript. The manuscript will undergo copyediting, typesetting, and review of the resulting proof before it is published in its final form. Please note that during the production process errors may be discovered which could affect the content, and all legal disclaimers that apply to the journal pertain.

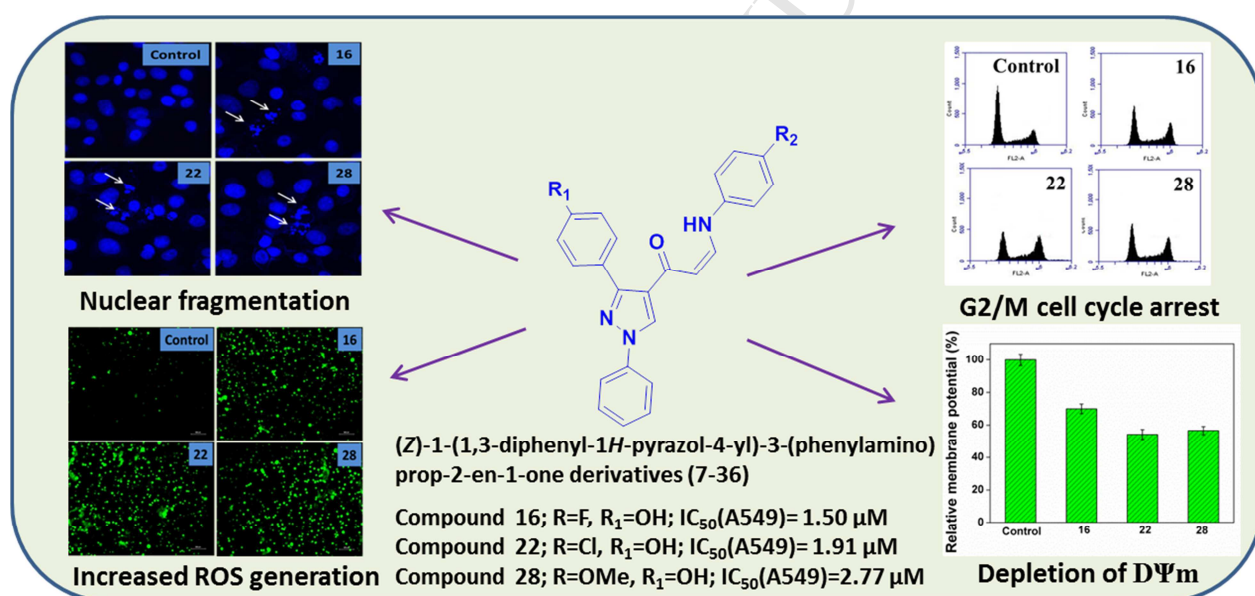
Graphical Abstract**Synthesis of (Z)-1-(1,3-diphenyl-1H-pyrazol-4-yl)-3-(phenylamino)prop-2-en-1-one derivatives as potential anticancer and apoptosis inducing agents**

T. Srinivasa Reddy,^{a,b,c} V. Ganga Reddy,^a Hitesh Kulhari,^{a,b,c} Ravi Shukla,^{c,d} Ahmed Kamal,^{a,b*} Vipul Bansal^{c*}

^aMedicinal Chemistry and Pharmacology, ^bIICT-RMIT Research Centre, CSIR-Indian Institute of Chemical Technology, Hyderabad, 500007, India

^cIan Potter NanoBioSensing Facility, Nano Biotechnology Research Laboratory, School of Science, RMIT University, Melbourne, VIC 3000, Australia

^dCentre for Advanced Materials and Industrial Chemistry, School of Science, RMIT University, Melbourne, VIC 3000, Australia



Synthesis of (Z)-1-(1,3-diphenyl-1H-pyrazol-4-yl)-3-(phenylamino)prop-2-en-1-one derivatives as potential anticancer and apoptosis inducing agents

T. Srinivasa Reddy,^{a,b,c} V. Ganga Reddy,^a Hitesh Kulhari,^{a,b,c} Ravi Shukla,^{c,d} Ahmed Kamal,^{a,b*} Vipul Bansal^{c*}

^a*Medicinal Chemistry and Pharmacology, ^bIICT-RMIT Research Centre, CSIR-Indian Institute of Chemical Technology, Hyderabad, 500007, India*

^c*Ian Potter NanoBioSensing Facility, Nano Biotechnology Research Laboratory, School of Science, RMIT University, Melbourne, VIC 3000, Australia*

^d*Centre for Advanced Materials and Industrial Chemistry, School of Science, RMIT University, Melbourne, VIC 3000, Australia*

*Corresponding authors:

Prof. Vipul Bansal

School of Science, RMIT University
GPO Box 2476, Melbourne, VIC 3000 Australia
E-mail: vipul.bansal@rmit.edu.au

Dr. Ahmed Kamal

CSIR-Indian Institute of Chemical Technology,
Hyderabad, 500007, India
E-mail: ahmedkamal@iict.res.in

Abstract

A series of (*Z*)-1-(1,3-diphenyl-1*H*-pyrazol-4-yl)-3-(phenylamino)prop-2-en-1-one derivatives were synthesized and characterized by ¹H and ¹³C NMR, ESI-MS and HRMS. All the synthesized compounds were evaluated for their anticancer activity against HT-29, PC-3, A549 and U87MG human tumor cell lines. Most of the synthesized compounds displayed potent growth inhibition selectively on A549 cancer cells and did not show significant toxicity to the non-cancerous HaCaT cells. Some of the representative compounds, particularly, **16**, **22** and **28** exhibited potent growth inhibition with IC₅₀ values in the range of 1.25-3.98 μM, which are comparable or even better than the standard chemotherapeutic drug 5-fluorouracil. Preliminary mechanistic studies revealed that these compounds could effectively inhibit the migration ability of A549 cells. Flow-cytometry analysis revealed that the compounds treatment led to G2/M cell cycle arrest. Moreover, the compounds induced apoptosis in A549 cells through depolarization of mitochondrial membrane potential (DΨ_m) and increased reactive oxygen species (ROS) production, suggesting their potential to act as promising lead compounds for the development of cancer chemotherapeutics.

Keywords:

Pyrazole; anti-cancer activity; cell cycle; apoptosis

1.0 Introduction

Cancer is a global health issue, representing the second leading cause of deaths [1]. Although current cancer treatments help to reduce or eliminate cancerous cells from the body, the current therapies are not always effective, efficient and may often cause adverse effects. The available chemotherapeutic drugs face several limitations such as drug resistance, high systemic toxicity, complex syntheses, and isolation procedures [2]. Therefore, there is a need for the development of new anticancer agents which can overcome these problems.

Most of the chemotherapeutic agents act primarily by activating the cell death signaling pathways including apoptosis [3]. Apoptosis is a programmed cell death that plays a crucial role in the maintenance of tissue development and homeostasis. Generally, it is considered that apoptosis is a multi-step process and is mainly regulated under the control of pro- and anti-apoptotic proteins, such as the Bcl-2 and inhibitor of apoptosis protein (IAP) family members, and executed through caspases, death receptors and mitochondria-mediated apoptosis pathway [4]. Thus, deregulation of these processes results in several diseases including cancer. Therefore, development of novel chemotherapeutic agents that induce apoptosis in cancer cells has emerged as an attractive strategy in cancer drug discovery [5].

Recently there has been growing interest in investigations on pyrazole ring systems because of their diverse pharmacological activities including antibacterial, antifungal, anti-inflammatory, antioxidant and antitumor activities [6-11]. These derivatives occupy a unique position in drug discovery for the synthesis of pharmaceutically active compounds with good safety profiles [12]. Several studies have shown that pyrazoles owe their anticancer activity either to inhibition of the enzymes or to the generation of reactive oxygen species (ROS), leading to cellular apoptosis [13-14].

On the other hand, a large number of small molecules that contain arylaminoprop-2-en-1-ones have been reported for their anticancer activity [15-17]. Earlier, our group also reported the synthesis of 2-arylpyridine-arylpropenones [15] and (Z)-(arylamino)-pyrazolyl/isoxazolyl-2-propenones as anticancer and apoptosis inducing agents [16]. Further, other studies have demonstrated that incorporation of propen-1-one moiety in to the molecules result in compounds with promising anticancer activity. For instance, (Z)-1-aryl-3-arylamino-2-propen-1-one's derivatives displayed a remarkable cytotoxicity towards various cancer cell lines with potent anti-tubulin activity by arresting the cells at G2/M phase of cell cycle [17].

Based on these observations and our ongoing interest on pyrazole ring systems [18-19] in the search for new compounds with potent anti-cancer activities, it seemed interesting to synthesize compounds incorporating pyrazole ring and arylaminoprop-2-en-1-ones to explore their anticancer activities. Therefore in this work, we synthesized a series of (Z)-1-(1,3-diphenyl-1*H*-pyrazol-4-yl)-3-(phenylamino)prop-2-en-1-one derivatives and evaluated their anticancer activity.

2.0 Result and Discussions

2.1 Chemistry

The synthesis route for (Z)-1-(1,3-diphenyl-1*H*-pyrazol-4-yl)-3-(phenylamino)prop-2-en-1-one derivatives is illustrated in **Scheme 1**. The intermediate compounds, 1-(1,3-diphenyl-1*H*-pyrazol-4-yl)prop-2-en-1-one derivatives **6 (a-e)** were synthesized according to our previously reported literature methods [18]. Briefly, acetophenones **1 (a-e)** on condensation with phenyl hydrazine (**2**) in ethanol at refluxing condition for 3 h gave the corresponding acetophenone phenyl hydrazones **3 (a-e)** which underwent cyclization into corresponding 1,3-di-phenyl pyrazole carboxaldehydes **4 (a-e)** on Vilsmeier–Haack reaction with DMF-POCl₃

complex via the two step attack process by the complex; first at the CH₃ group of the substrate with the subsequent cyclization into 3-arylpyrazoles and then at the C₄ atom of the resulting heterocycles. These aldehyde intermediates **4 (a-e)** were reacted with ethynylmagnesium bromide in dry tetrahydrofuran (THF) at 0 °C to room temperature to produce alcohol substituted derivatives **5 (a-e)**. The secondary alcohols on oxidation with 2-iodoxybenzoic acid (IBX) in the presence of dimethyl sulfoxide (DMSO) gave 1-(1,3-diphenyl-1*H*-pyrazol-4-yl)prop-2-yn-1-one derivatives **6 (a-e)**. The final target compounds (*Z*)-1-(1,3-diphenyl-1*H*-pyrazol-4-yl)-3-(phenylamino)prop-2-en-1-one (**7-36**) were synthesized according to a previously reported method [17] which involves reaction of terminal alkyne substituted pyrazoles **6 (a-e)** with different substituted aryl amines in ethanol at room temperature. All the compounds were characterized by ¹H NMR, ¹³C, ESI-MS and HRMS (supplementary information).

< **Scheme 1** >

2.2 *In vitro* anticancer activity

All the synthesized compounds were investigated for their *in vitro* cytotoxicity against four human tumor cells HT-29 (colon), PC-3 (prostate), A549 (lung) and U87MG (glioblastoma) using standard MTT assay [20]. 5-fluorouracil (5-FU) was used as a standard reference compound and the results are summarized in **Table 1**. Close observation of results from **Table 1** indicated that almost all the synthesized derivatives were selectively cytotoxic to the A549 lung cancer cells. For instance, some of the compounds such as **10, 11, 16, 20, 22, 25, 26, 28, 34** displayed potent growth inhibition on A549 cells with IC₅₀ values in the range of 1.25-3.98 μM, which are comparable or even better than the standard 5-FU. The potent growth inhibitory activity was observed with the compound **16** (IC₅₀ - 1.5±0.45 μM), followed by the compounds **22** (IC₅₀ - 1.91±0.21 μM) and **28** (IC₅₀ - 2.77±0.24 μM) against

A549 cancer cells. The other three remaining tumor cell lines also displayed maximum sensitivity towards these compounds with IC_{50} values not more than 4.71 μ M. Compound **11** was highly active on HT-29 colon cancer cells (IC_{50} - 1.56 \pm 0.32 μ M), while the compounds **28** and **34** showed selective potency against PC-3 prostate cancer cells (IC_{50} - 1.98 \pm 0.16 μ M) and U87MG brain cancer cells (IC_{50} -1.8 \pm 0.57 μ M), respectively. When all the synthesized compounds were further tested on non-cancerous human HaCaT cells, most of these did not exhibit cytotoxicity, which indicates the selectivity of these compounds towards cancer cells. The most active compounds **16**, **22** and **28** displayed moderate growth inhibition of HaCaT cells with IC_{50} in the range of 16.2-34.6 μ M. These are about 10-12 times less toxic than that of A549 lung cancer cell growth inhibition values.

< Table 1 >

Structure-activity relationship (SAR) could be observed by examining the effect of substituents such as fluorine, chlorine, trifluoromethyl and methoxy in A and B phenyl rings of these derivatives on cell growth inhibition. It was noted that strong electron donating group (OH) on the aromatic B ring produced the compounds (**10**, **16**, **22**, **28** and **34**) with potent and broad spectrum of activity on all the tested cancer cell lines with IC_{50} values in the range of 1.35-3.21 μ M. Further, the other electron donating groups such as methoxy (**11**, **17**, **23**, **29** and **35**) and 3,4,5-methoxy (**12**, **18**, **24**, **30** and **36**) substitutions also resulted in compounds with remarkable cytotoxicity. In contrast, the compounds with electron withdrawing substitutions chloro (**8**, **14**, **20**, **26** and **32**) and trifluoromethyl (**9**, **15**, **21**, **27** and **33**) on B ring displayed no cytotoxicity on cancer cells. It should be noted that different substitutions on the aryl A ring didn't have any significant role in activity. The interesting biological activity of compounds **16**, **22** and **28** prompted us to investigate their effects at cellular level and in particular, the mechanisms responsible for cell death.

2.3 *In vitro* cell migration assay

The mortality and prognosis in cancer patients correlate with metastatic potential of tumors. As cell motility and migration associate with the metastatic behavior of cancer cells, we investigated the effect of selected potent compounds on A549 cell migration capability using wound healing assay [21]. To achieve this, A549 cells were independently treated with compounds **16**, **22** and **28** after creating the wounds/scratch in the confluent monolayers of cultured cells. Images of wounded areas were captured after 0 h, 24 h and 48 h of compound treatments. **Figure 1** shows that almost complete healing of wounded area was observed in control cells after 48 h, whereas the healing was strongly inhibited in the cells treated with compounds, thereby reflecting the ability of these compounds to inhibit the migration capability of the cells. The compound **22** displayed strongest cellular migration inhibition ability, followed by compounds **28** and **16**.

< **Figure 1** >

2.4 Effect on actin polymerisation

Directional migration or motility of cancer cells is initiated by changes in cell polarity, remodelling of cytoskeleton and regulation of microtubules and actin [22]. It is established that the localized polymerisation of actin filaments is the driving force for cellular motility [23]. As tested compounds inhibited the migration of A549 cancer cells, it was of interest to further investigate their effect on actin polymerisation. The formation of actin cytoskeleton was assessed by staining the cells with rhodamine-phalloidin [24], which specifically binds to F-actin. The results from the **Figure 2** demonstrate that all the three compounds disrupted the actin fibre assembly which is more prominent with the compound **22**. The cells treated with the compounds displayed disappearance of F-actin extensions. This loss of F-actin extensions at the periphery of the cell membrane resulted in loss of migration ability of the cancer cells.

Collectively, these results demonstrate that the compounds **16**, **22** and **28** inhibit the migration potential of A549 lung cancer cells, at least in part through disrupting F-actin assembly.

< **Figure 2** >

2.5 Cell cycle analysis

To further investigate the mechanism of cell growth inhibition, we examined the effect of these compounds on cell cycle progression using propidium iodide staining [25]. Cell cycle phase distribution analysis, as studied using flow cytometry, demonstrated that treatment of A549 cells with compounds **16**, **22** and **28** resulted in significant increase in the DNA content in G2/M phase and subsequent reduction in G1 phase of the cell cycle (**Figure 3**). The percentage of cells in the G2/M phase after the treatment with the compounds **16**, **22** and **28** were 41%, 49.2% and 43.1%, respectively, in comparison to the control (27.2%). These results demonstrate that the compound-induced G2/M phase of cell cycle arrest may be one of the possible mechanisms of cell growth inhibition.

< **Figure 3** >

2.6 Apoptosis studies

After G2/M arrest, many of the tumor cells, for instance lung cancer cells, exhibit morphologic changes consistent with apoptosis, i.e., membrane blebbing, the appearance of a rounded morphology, and eventually detachment from the surface of the tissue culture dish [26]. It has been previously suggested that G2/M cell cycle arrest leads to apoptosis in a number of cancer cell lines [27-28]. Therefore it was considered of interest to examine the apoptosis inducing effect of these active compounds in A549 cells.

2.6.1 Hoechst Staining

To investigate the apoptosis inducing effect of these compounds on the basis of morphological changes of the cellular nucleus, we carried out a Hoechst staining assay. Hoechst 33242 is a cell permeable, fluorescent nucleus staining dye that stains apoptotic cells as bright blue because of nuclear condensation [29]. A549 cells were incubated with the compounds **16**, **22** and **28** for 24 h and stained with Hoechst 33242. **Figure 4** shows that the compound-treated cells reflect distinct pattern of morphological features such as chromatin condensation and nuclear fragmentation (as indicated by arrowheads), which are typical hallmarks of apoptosis; whereas the untreated control cells displayed uniform rounded nucleus. Compounds **16**, **22** and **28** induced varying degrees of apoptosis with compounds **22** being the strongest inducer of morphologic changes characteristic of apoptosis in A549 cells.

< **Figure 4** >

2.6.2 Effect on mitochondrial membrane potential ($D\Psi_m$)

Maintenance of mitochondrial membrane potential is essential for mitochondrial integrity and cellular bioenergetics [30]. Loss of mitochondrial membrane functions results in release of cytochrome C into the cytosol, which leads to apoptosis. Therefore, to investigate the effect of these compounds on $D\Psi_m$, we carried out rhodamine 123 staining [31]. Mitochondria that maintain normal $D\Psi_m$ retain the rhodamine fluorescence, whereas depolarised mitochondria are unable to retain the rhodamine that results in loss of rhodamine green fluorescence. Thus, the loss of $D\Psi_m$ can be monitored by a shift in green fluorescence intensity. As shown in **Figure 5**, cells treated with the compounds **16**, **22** and **28** displayed a significant 30-46% loss of $D\Psi_m$ in comparison to the untreated cells. Among these, compounds **22** and **28** induced 45.8 and 43.5% loss of $D\Psi_m$, respectively, followed by the compound **16** (30%). This suggests that the compounds are able to induce apoptosis through the collapse of mitochondrial membrane potential in A549 lung cancer cells.

< Figure 5 >

2.6.3 Effect on intracellular reactive oxygen species (ROS) levels

Reactive oxygen species are reported to be involved in early stages of apoptosis in many cellular systems. Further, decrease in $D\Psi_m$ typically damages mitochondrial electron transport chain, which results in elevation of intracellular ROS [32]. To determine whether this event occurs during apoptosis induction by our compounds, we examined intracellular ROS production using DCFDA. DCFDA is a cell permeable non-fluorescent dye, which upon oxidation by intracellular esterases, converts into a green fluorescent DCF. Therefore, the increase in green fluorescence intensity represents the increased production of ROS. **Figure 6** indicates that cells treated with the compounds **16**, **22** and **28** display significantly higher green fluorescence intensity compared to the untreated cells. Quantitative analysis by fluorescence spectrofluorimetry revealed that the compounds treatment resulted in 2.1-2.8 fold increase in green fluorescence intensity, which suggests that elevated intracellular ROS levels may also play an important role in the cytotoxicity and apoptosis induced by these compounds.

< Figure 6 >

3.0 Conclusion

In the present work, a series of (*Z*)-1-(1,3-diphenyl-1*H*-pyrazol-4-yl)-3-(phenylamino)prop-2-en-1-one derivatives were synthesized and evaluated for their anticancer activity against four human tumor cells and an additional non-cancerous cell. The compounds **16**, **22** and **28** displayed potent and broad spectrum of growth inhibition on all the tested cancer cells. The SAR study demonstrated that electron donating groups at *para* position of aromatic B ring is essential for the activity of these derivatives, which led to the selection of the most active

compounds in the series. The compounds inhibit the *in vitro* cellular migration of A549 lung cancer cells through disruption of cytoskeleton. Further biological assessments of **16**, **22** and **28** revealed that these compounds trigger cell cycle arrest in G2/M phase and induce apoptosis through depolarization of mitochondrial membrane potential and through enhanced production of ROS in lung cancer cells. These findings suggest that (Z)-1-(1,3-diphenyl-1H-pyrazol-4-yl)-3-(phenylamino)prop-2-en-1-one derivatives offer promising leads for the further development of anticancer agents.

4.0 Experimental Section

All the reagents and solvents were of commercial grade and used as received. The progress of the reactions was monitored by thin layer chromatography (TLC) performed on silica gel glass plates containing 60 F-254, and visualization on TLC was achieved by UV light or iodine indicator. Melting points were measured with an Electro-thermal melting point apparatus, and are uncorrected. ^1H and ^{13}C NMR spectra were recorded on INOVA (400 MHz) or Gemini Varian-VXR-Unity (200 MHz) or Bruker UXNMR/XWIN-NMR (300 MHz) instruments. ESI spectra were recorded on Micro mass, Quattro LC using ESI+ software with capillary voltage of 3.98 kV and ESI mode positive ion trap detector.

4.1 General procedure for the synthesis of 1-(1,3-diphenyl-1H-pyrazol-4-yl)prop-2-yn-1-one derivatives (**6a-e**)

The 1,3-diphenyl-1H-pyrazole-4-carboxaldehydes (**4a-e**), 1-(1,3-diphenyl-1H-pyrazol-4-yl)prop-2-yn-1-ol derivatives (**5a-e**), and their corresponding oxidation products 1-(1,3-diphenyl-1H-pyrazol-4-yl)prop-2-yn-1-one derivatives (**6a-e**) were synthesized according to our previously reported methods [14, 15].

4.2 General synthesis of (Z)-1-(1,3-diphenyl-1H-pyrazol-4-yl)-3-((4-fluorophenyl)amino)prop-2-en-1-ones

To a solution of ethynylketones **6a-e** (1 mmol) in absolute ethanol, different substituted arylamines (1 mmol) were added at room temperature and the reaction was continued for 4 h at room temperature. After the completion of reaction (checked by TLC), the mixture was diluted with water and the products were filtered. The obtained crude products (**7-36**) were purified through column chromatography using Hexane/Ethyl acetate as eluent system.

4.2.1 (Z)-1-(1,3-diphenyl-1H-pyrazol-4-yl)-3-((4-fluorophenyl)amino)prop-2-en-1-one (**7**)

Light Brown solid, yield 74%, mp: 164-166 °C; ¹H NMR (300 MHz, CDCl₃) δ 11.92 (d, *J* = 12.0 Hz, 1H), 8.45 (s, 1H), 7.87 – 7.67 (m, 4H), 7.56 – 7.43 (m, 4H), 7.41 – 7.30 (m, 2H), 7.28 (s, 1H), 7.21 (dd, *J* = 12.0, 7.8 Hz, 1H), 7.00 (m, 3H), 5.51 (d, *J* = 7.7 Hz, 1H). ¹³C NMR (75 MHz, CDCl₃) δ 186.2, 160.7, 157.5, 152.6, 144.3, 139.4, 136.6, 133.0, 130.0, 129.5, 128.5, 128.2, 127.1, 123.9, 119.4, 117.7, 116.6, 116.3, 96.7. MS (ESI): 384 [M+H]⁺; HRMS (ESI) calculated for C₂₄H₁₉ON₃F [M+H]⁺; 384.15067; found: 384.15110.

4.2.2 (Z)-3-((4-chlorophenyl)amino)-1-(1,3-diphenyl-1H-pyrazol-4-yl)prop-2-en-1-one (**8**)

White solid, yield 77%, mp: 196-198 °C; ¹H NMR (300 MHz, CDCl₃) δ 11.89 (d, *J* = 12.1 Hz, 1H), 8.45 (s, 1H), 7.87 – 7.72 (m, 4H), 7.55 – 7.44 (m, 5H), 7.36 (t, *J* = 7.4 Hz, 1H), 7.32 – 7.25 (m, 2H), 7.19 (s, 1H), 7.02 – 6.94 (m, 2H), 5.53 (d, *J* = 7.9 Hz, 1H). ¹³C NMR (75 MHz, CDCl₃) δ 186.4, 152.7, 143.4, 139.4, 139.0, 133.0, 130.0, 129.7, 129.5, 129.5, 128.6, 128.4, 128.2, 127.2, 124.0, 119.4, 117.2, 97.3. MS (ESI): 400 [M+H]⁺; HRMS (ESI) calculated for C₂₄H₁₉ON₃Cl [M+H]⁺; 400.12112; found: 400.12131.

4.2.3 (Z)-1-(1,3-diphenyl-1H-pyrazol-4-yl)-3-((4-(trifluoromethyl)phenyl)amino)prop-2-en-1-one (9)

Pale yellow solid, yield 68%, mp: 145-148 °C; ¹H NMR (300 MHz, CDCl₃) δ 11.83 (d, *J* = 12.0 Hz, 1H), 8.36 (s, 1H), 7.76-7.63 (m, 4H), 7.48 (d, *J* = 8.5 Hz, 2H), 7.45 – 7.32 (m, 5H), 7.28 (d, *J* = 7.3 Hz, 1H), 7.18 (dd, *J* = 7.1, 4.8 Hz, 1H), 7.00 (d, *J* = 8.4 Hz, 2H), 5.50 (d, *J* = 8.0 Hz, 1H). ¹³C NMR (75 MHz, CDCl₃) δ 186.7, 152.8, 143.2, 142.5, 139.3, 132.9, 130.2, 129.5, 128.7, 128.2, 127.3, 127.1, 125.9, 125.1, 124.7, 123.8, 119.5, 115.5, 98.3. MS (ESI): 434 [M+H]⁺; HRMS (ESI) calculated for C₂₅H₁₉ON₃F₃ [M+H]⁺; 434.14747 found: 434.14636.

4.2.4 (Z)-1-(1,3-diphenyl-1H-pyrazol-4-yl)-3-((4-hydroxyphenyl)amino)prop-2-en-1-one (8)

Brown solid, yield 81%, mp: 157-159 °C; ¹H NMR (300 MHz, CDCl₃) δ 11.89 (d, *J* = 12.2 Hz, 1H), 8.41 (s, 1H), 7.81-7.69 (m, 4H), 7.45 (t, *J* = 7.6 Hz, 2H), 7.31 (t, *J* = 7.4 Hz, 1H), 7.19 (dd, *J* = 11.9, 7.6 Hz, 1H), 7.00 (d, *J* = 8.6 Hz, 2H), 6.81 (d, *J* = 8.7 Hz, 2H), 6.77 (d, *J* = 8.7 Hz, 2H), 5.49 (d, *J* = 7.8 Hz, 1H). ¹³C NMR (75 MHz, CDCl₃+DMSO-*d*₆) δ 184.4, 153.2, 151.3, 144.3, 138.4, 132.2, 131.5, 129.1, 128.6, 128.4, 127.1, 126.1, 123.0, 118.1, 116.9, 115.5, 94.6. MS (ESI): 382 [M+H]⁺; HRMS (ESI) calculated for C₂₄H₂₀O₂N₃ [M+H]⁺; 382.15500; found: 382.15557.

4.2.5 (Z)-1-(1,3-diphenyl-1H-pyrazol-4-yl)-3-((4-methoxyphenyl)amino)prop-2-en-1-one (11)

Brown solid, yield 82%, mp: 139-141 °C; ¹H NMR (300 MHz, CDCl₃) δ 11.84 (d, *J* = 11.8 Hz, 1H), 8.36 (s, 1H), 7.78-7.62 (m, 4H), 7.51-7.38 (m, 5H), 7.30 – 7.02 (m, 2H), 6.92 (d, *J* = 8.4 Hz, 2H), 6.79 (d, *J* = 8.2 Hz, 2H), 5.36 (d, *J* = 7.5 Hz, 1H), 3.70 (s, 3H). ¹³C NMR (75

MHz, CDCl₃) δ 185.8, 156.2, 152.5, 145.0, 139.4, 133.8, 133.1, 129.8, 129.5, 128.5, 128.2, 127.1, 124.2, 119.4, 117.8, 114.9, 96.0, 55.5. MS (ESI): 396 [M+H]⁺; HRMS (ESI) calculated for C₂₅H₂₂O₂N₃ [M+H]⁺; 396.17065; found: 396.17065.

4.2.6 (Z)-1-(1,3-diphenyl-1H-pyrazol-4-yl)-3-((3,4,5-trimethoxyphenyl)amino)prop-2-en-1-one (12)

Brown solid, yield 75%, mp: 152-154 °C; ¹H NMR (300 MHz, CDCl₃) δ 11.93 (d, *J* = 12.1 Hz, 1H), 8.46 (d, *J* = 7.8 Hz, 1H), 7.89-7.76 (m, 4H), 7.57 – 7.41 (m, 5H), 7.36 (t, *J* = 7.3 Hz, 1H), 7.27 – 7.20 (m, 1H), 6.28 (s, 2H), 5.51 (d, *J* = 7.8 Hz, 1H), 3.87 (s, 6H), 3.83 (s, 3H). ¹³C NMR (75 MHz, CDCl₃) δ 186.0, 154.1, 152.7, 144.1, 139.4, 136.5, 134.5, 133.1, 129.8, 129.5, 128.7, 128.3, 127.2, 124.0, 119.4, 96.5, 93.8, 61.0, 56.1. MS (ESI): 456 [M+H]⁺; HRMS (ESI) calculated for C₂₇H₂₆O₄N₃ [M+H]⁺; 456.19178; found: 456.19088.

4.2.7 (Z)-1-(3-(4-fluorophenyl)-1-phenyl-1H-pyrazol-4-yl)-3-((4-fluorophenyl)amino)prop-2-en-1-one (13)

Pale yellow, yield 77%, mp: 196-198 °C; ¹H NMR (500 MHz, CDCl₃) δ 11.89 (d, *J* = 12.0 Hz, 1H), 8.42 (s, 1H), 7.81-7.69 (m, 4H), 7.57-7.48 (m, 2H), 7.41 (d, *J* = 8.2 Hz, 2H), 7.39 (t, *J* = 7.3 Hz, 1H), 7.23 – 7.18 (m, 1H), 6.99 (dd, *J* = 10.6, 6.4 Hz, 4H), 5.48 (d, *J* = 7.8 Hz, 1H). ¹³C NMR (75 MHz, CDCl₃) δ 185.8, 161.9, 157.4, 151.4, 144.6, 139.2, 136.5, 134.6, 131.5, 130.7, 130.1, 128.4, 127.5, 123.9, 119.4, 117.7, 116.6, 116.3, 96.4. MS (ESI): 402 [M+H]⁺; HRMS (ESI) calculated for C₂₄H₁₈ON₃F₂ [M+H]⁺; 402.14125; found: 402.14100.

4.2.8 (Z)-3-((4-chlorophenyl)amino)-1-(3-(4-fluorophenyl)-1-phenyl-1H-pyrazol-4-yl)prop-2-en-1-one (14)

Light yellow solid, yield 70%, mp: 157-159 °C; ¹H NMR (300 MHz, CDCl₃) δ 11.87 (d, *J* = 12.1 Hz, 1H), 8.42 (s, 1H), 7.86 – 7.72 (m, 3H), 7.51 (t, *J* = 7.8 Hz, 2H), 7.37 (t, *J* = 7.4 Hz,

1H), 7.29 (dt, $J = 8.5, 5.2$ Hz, 4H), 7.21 – 7.13 (m, 2H), 7.08-7.01 (m, 2H), 5.55 (d, $J = 7.9$ Hz, 1H). ^{13}C NMR (75 MHz, CDCl_3) δ 185.9, 151.8, 143.5, 139.3, 138.9, 131.3, 131.2, 130.0, 129.7, 129.6, 129.0, 128.5, 127.3, 123.7, 119.4, 117.3, 115.3, 115.0, 97.0. MS (ESI): 418 $[\text{M}+\text{H}]^+$; HRMS (ESI) calculated for $\text{C}_{24}\text{H}_{18}\text{ON}_3\text{ClF}$ $[\text{M}+\text{H}]^+$; 418.11169; found: 418.11105.

4.2.9 (Z)-1-(3-(4-fluorophenyl)-1-phenyl-1H-pyrazol-4-yl)-3-((4-(trifluoromethyl)phenyl)amino)prop-2-en-1-one (15)

Brown solid, yield 66%, mp: 168-171 °C; ^1H NMR (300 MHz, CDCl_3) δ 11.89 (d, $J = 12.0$ Hz, 1H), 8.43 (s, 1H), 7.85–7.66 (m, 5H), 7.57-7.43 (m, 3H), 7.18 (d, $J = 8.6$ Hz, 2H), 7.07-6.99 (m, 2H), 6.81 (d, $J = 8.7$ Hz, 2H), 5.59 (d, $J = 7.9$ Hz, 1H). ^{13}C NMR (75 MHz, CDCl_3) δ 187.7, 160.3, 153.3, 152.7, 142.3, 139.1, 135.3, 130.7, 129.5, 127.9, 127.2, 127.1, 123.9, 122.3, 119.8, 119.4, 115.5, 113.6, 81.6. MS (ESI): 452 $[\text{M}+\text{H}]^+$; HRMS (ESI) calculated for $\text{C}_{25}\text{H}_{18}\text{ON}_3\text{F}_4$ $[\text{M}+\text{H}]^+$ 452.13824; found: 452.13828.

4.2.10 (Z)-1-(3-(4-fluorophenyl)-1-phenyl-1H-pyrazol-4-yl)-3-((4-hydroxyphenyl)amino)prop-2-en-1-one (16)

Brown solid, yield 71%, mp: 191-193 °C; ^1H NMR (300 MHz, CDCl_3) δ 11.91 (d, $J = 12.1$ Hz, 1H), 8.43 (s, 1H), 7.78 – 7.76 (m, 4H), 7.47 (t, $J = 8.0$ Hz, 2H), 7.36 (t, $J = 7.3$ Hz, 1H), 7.17-7.03 (m, 3H), 6.78 (d, $J = 8.9$ Hz, 2H), 6.63-6.54 (m, 2H) 5.51 (d, $J = 7.8$ Hz, 1H). ^{13}C NMR (75 MHz, $\text{CDCl}_3+\text{DMSO}-d_6$) δ 184.1, 163.3, 160.1, 153.1, 150.3, 144.3, 138.2, 131.3, 130.1, 129.0, 128.5, 128.3, 126.0, 122.6, 117.9, 116.8, 115.4, 113.9, 113.7, 94.2. MS (ESI): 400 $[\text{M}+\text{H}]^+$; HRMS (ESI) calculated for $\text{C}_{24}\text{H}_{19}\text{O}_2\text{N}_3\text{F}$ $[\text{M}+\text{H}]^+$; 400.14558; found: 400.14553

4.2.11 (Z)-1-(3-(4-fluorophenyl)-1-phenyl-1H-pyrazol-4-yl)-3-((4-methoxyphenyl)amino)prop-2-en-1-one (17)

Yellow solid, yield 73%, mp: 149-151 °C; ¹H NMR (300 MHz, CDCl₃) δ 11.92 (d, *J* = 12.3 Hz, 1H), 8.42 (s, 1H), 7.85 – 7.73 (m, 5H), 7.51 (t, *J* = 7.8 Hz, 2H), 7.36 (t, *J* = 7.4 Hz, 1H), 7.17 (t, *J* = 8.7 Hz, 2H), 7.03 (d, *J* = 9.0 Hz, 2H), 6.89 (d, *J* = 8.9 Hz, 2H), 5.48 (d, *J* = 7.7 Hz, 1H), 3.81 (s, 3H). ¹³C NMR (75 MHz, CDCl₃) δ 185.6, 164.7, 156.3, 151.6, 145.0, 139.4, 133.8, 131.3, 131.2, 129.8, 129.5, 127.2, 123.9, 119.4, 117.8, 115.3, 115.0, 95.7, 55.5. MS (ESI): 414 [M+H]⁺; HRMS (ESI) calculated for C₂₅H₂₁O₂N₃F [M+H]⁺ 414.16103; found: 414.16103.

4.2.12 (Z)-1-(3-(4-fluorophenyl)-1-phenyl-1H-pyrazol-4-yl)-3-((3,4,5-trimethoxyphenyl)amino)prop-2-en-1-one (18)

Yellow solid, yield 79%, mp: 147-149 °C; ¹H NMR (300 MHz, CDCl₃) δ 11.90 (d, *J* = 12.2 Hz, 1H), 8.42 (s, 1H), 7.82-7.75 (m, 4H), 7.51 (t, *J* = 7.8 Hz, 2H), 7.37 (t, *J* = 7.4 Hz, 1H), 7.33 – 7.23 (m, 1H), 7.16-7.07 (m, 2H), 6.29 (s, 2H), 5.53 (d, *J* = 7.8 Hz, 1H), 3.87 (s, 6H), 3.83 (s, 3H). ¹³C NMR (75 MHz, CDCl₃) δ 185.8, 154.1, 151.8, 144.3, 139.3, 136.4, 134.5, 131.3, 129.8, 129.5, 129.1, 127.3, 123.7, 119.4, 115.3, 115.0, 96.2, 93.9, 61.0, 56.2. MS (ESI): 474 [M+H]⁺; HRMS (ESI) calculated for C₂₇H₂₅O₄N₃F [M+H]⁺; 474.18236; found: 474.18135.

4.2.13 (Z)-1-(3-(4-chlorophenyl)-1-phenyl-1H-pyrazol-4-yl)-3-((4-fluorophenyl)amino)prop-2-en-1-one (19)

Yellow solid, yield 68%, mp: 153-155 °C; ¹H NMR (500 MHz, CDCl₃) δ 11.87 (d, *J* = 12.2 Hz, 1H), 8.40 (s, 1H), 7.78-7.61 (m, 4H), 7.52-7.47 (m, 2H), 7.43 (d, *J* = 8.4 Hz, 2H), 7.36 (t, *J* = 7.4 Hz, 1H), 7.25–7.21 (m, 1H), 7.04 (dd, *J* = 10.6, 6.4 Hz, 4H), 5.52 (d, *J* = 7.8 Hz, 1H).

^{13}C NMR (75 MHz, CDCl_3) δ 185.8, 160.8, 157.5, 151.5, 144.6, 139.3, 136.5, 134.6, 131.4, 130.7, 129.9, 129.6, 128.4, 127.4, 123.9, 119.4, 117.7, 116.6, 116.3, 96.5. MS (ESI): 418 $[\text{M}+\text{H}]^+$; HRMS (ESI) calculated for $\text{C}_{24}\text{H}_{18}\text{ON}_3\text{ClF}$ $[\text{M}+\text{H}]^+$; 418.11169; found: 418.11110.

4.2.14 **(Z)-1-(3-(4-chlorophenyl)-1-phenyl-1H-pyrazol-4-yl)-3-((4-chlorophenyl)amino)prop-2-en-1-one (20)**

Pale yellow solid, yield 71%, mp: 176-178 °C; ^1H NMR (500 MHz, CDCl_3) δ 11.85 (d, $J = 12.2$ Hz, 1H), 8.40 (s, 1H), 7.79–7.71 (m, 4H), 7.55–7.46 (m, 2H), 7.46–7.42 (m, 2H), 7.36 (t, $J = 7.4$ Hz, 1H), 7.30–7.28 (m, 2H), 7.24 (s, 1H), 6.99 (dd, $J = 9.2, 2.4$ Hz, 2H), 5.54 (d, $J = 7.9$ Hz, 1H). ^{13}C NMR (75 MHz, CDCl_3) δ 185.8, 151.1, 144.3, 139.5, 136.6, 134.9, 131.4, 130.7, 129.8, 129.6, 128.2, 127.6, 127.4, 123.9, 119.8, 117.7, 116.5, 116.3, 95.8. MS (ESI): 434 $[\text{M}+\text{H}]^+$; HRMS (ESI) calculated for $\text{C}_{24}\text{H}_{18}\text{ON}_3\text{Cl}_2$ $[\text{M}+\text{H}]^+$ 434.08214; found: 434.08242.

4.2.15 **(Z)-1-(3-(4-chlorophenyl)-1-phenyl-1H-pyrazol-4-yl)-3-((4-(trifluoromethyl)phenyl)amino)prop-2-en-1-one (21)**

Pale yellow solid, yield 78%, mp: 183-185 °C; ^1H NMR (300 MHz, CDCl_3) δ 11.87 (d, $J = 12.1$ Hz, 1H), 8.42 (s, 1H), 7.81–7.68 (m, 4H), 7.57–7.43 (m, 2H), 7.38–7.28 (m, 2H), 7.19 (d, $J = 8.6$ Hz, 2H), 7.11–7.03 (m, 2H), 6.83 (d, $J = 8.6$ Hz, 2H), 5.56 (d, $J = 7.8$ Hz, 1H). ^{13}C NMR (75 MHz, CDCl_3) δ 187.9, 152.8, 142.3, 139.2, 135.3, 130.9, 129.8, 128.1, 127.8, 127.5, 123.9, 122.3, 119.8, 119.4, 115.5, 113.6, 81.9. MS (ESI): 468 $[\text{M}+\text{H}]^+$; HRMS (ESI) calculated for $\text{C}_{25}\text{H}_{18}\text{ON}_3\text{F}_3\text{Cl}$ $[\text{M}+\text{H}]^+$ 468.10900; found: 468.10911.

4.2.16 **(Z)-1-(3-(4-chlorophenyl)-1-phenyl-1H-pyrazol-4-yl)-3-((4-hydroxyphenyl)amino)prop-2-en-1-one (22)**

Yellow solid, yield 69%, mp: 158-160 °C; ^1H NMR (500 MHz, CDCl_3) δ 11.89 (d, $J = 12.1$ Hz, 1H), 8.42 (s, 1H), 7.89–7.78 (m, 2H), 7.55–7.53 (m, 3H), 7.47–7.41 (m, 2H), 7.37 (t, $J = 7.4$ Hz, 1H), 7.18–7.09 (m, 2H), 7.01 (s, 1H), 6.53 (d, $J = 8.2$ Hz, 2H), 5.57 (d, $J = 7.8$ Hz, 1H). ^{13}C NMR (75 MHz, $\text{CDCl}_3+\text{DMSO-}d_6$) δ 184.1, 153.2, 150.2, 144.5, 138.3, 133.1, 131.4, 130.8, 129.8, 129.1, 128.6, 127.1, 126.2, 122.8, 118.2, 116.9, 115.5, 94.3. MS (ESI): 416 $[\text{M}+\text{H}]^+$; HRMS (ESI) calculated for $\text{C}_{24}\text{H}_{19}\text{O}_2\text{N}_3\text{Cl}$ $[\text{M}+\text{H}]^+$ 416.11603; found: 416.11562.

4.2.17 **(Z)-1-(3-(4-chlorophenyl)-1-phenyl-1H-pyrazol-4-yl)-3-((4-methoxyphenyl)amino)prop-2-en-1-one (23)**

Pale yellow solid, yield 71%, mp: 178-180 °C; ^1H NMR (300 MHz, CDCl_3) δ 11.89 (d, $J = 12.0$ Hz, 1H), 8.42 (s, 1H), 7.81–7.69 (m, 4H), 7.53 (t, $J = 7.8$ Hz, 2H), 7.38 (d, $J = 7.6$ Hz, 2H), 7.36–7.28 (m, 4H), 7.00 (t, $J = 8.4$ Hz, 2H), 5.51 (d, $J = 7.9$ Hz, 1H), 3.87 (s, 3H). ^{13}C NMR (75 MHz, CDCl_3) δ 186.4, 153.4, 143.5, 143.2, 139.4, 139.1, 138.9, 130.6, 129.9, 129.7, 129.3, 128.6, 127.2, 125.3, 123.7, 119.4, 117.4, 117.2, 113.5, 97.5, 55.3. MS (ESI): 430 $[\text{M}+\text{H}]^+$; HRMS (ESI) calculated for $\text{C}_{25}\text{H}_{21}\text{O}_2\text{N}_3\text{Cl}$ $[\text{M}+\text{H}]^+$ 430.13168; found: 430.13107.

4.2.18 **(Z)-1-(3-(4-chlorophenyl)-1-phenyl-1H-pyrazol-4-yl)-3-((3,4,5-trimethoxyphenyl)amino)prop-2-en-1-one (24)**

Pale yellow solid, yield 76%, mp: 171-173 °C; ^1H NMR (500 MHz, CDCl_3) δ 11.88 (d, $J = 12.2$ Hz, 1H), 8.40 (s, 1H), 7.81–7.69 (m, 4H), 7.50 (t, $J = 7.9$ Hz, 2H), 7.44 (d, $J = 8.4$ Hz, 2H), 7.36 (t, $J = 7.4$ Hz, 1H), 7.28 (dd, $J = 9.8, 5.3$ Hz, 1H), 6.28 (s, 2H), 5.51 (d, $J = 7.8$ Hz, 1H), 3.85 (s, 6H), 3.81 (s, 3H). ^{13}C NMR (75 MHz, CDCl_3) δ 185.8, 154.1, 151.6, 144.4, 139.3, 136.4, 134.6, 134.5, 131.4, 130.7, 129.9, 129.5, 128.5, 127.4, 123.8, 119.4, 96.2, 93.8,

61.0, 56.2. MS (ESI): 490 [M+H]⁺; HRMS (ESI) calculated for C₂₇H₂₅O₄N₃Cl [M+H]⁺ 490.15236; found: 490.15258.

4.2.19 (Z)-3-((4-fluorophenyl)amino)-1-(3-(4-methoxyphenyl)-1-phenyl-1H-pyrazol-4-yl)prop-2-en-1-one (25)

Yellow solid, yield 82%, mp: 169-171 °C; ¹H NMR (300 MHz, CDCl₃) δ 11.91 (d, *J* = 12.2 Hz, 1H), 8.43 (s, 1H), 7.80 (d, *J* = 7.8 Hz, 2H), 7.72 (dd, *J* = 9.2, 2.3 Hz, 2H), 7.50 (t, *J* = 7.9 Hz, 2H), 7.36 (t, *J* = 7.4 Hz, 1H), 7.22 (dd, *J* = 12.3, 7.9 Hz, 1H), 7.07-6.97 (m, 6H), 5.54 (d, *J* = 7.8 Hz, 1H), 3.89 (s, 3H). ¹³C NMR (75 MHz, CDCl₃) δ 185.2, 158.9, 151.3, 143.5, 138.4, 135.8, 129.7, 129.3, 128.6, 126.2, 124.4, 122.5, 118.2, 116.7, 115.6, 115.3, 112.6, 95.7, 54.3. MS (ESI): 414 [M+H]⁺; HRMS (ESI) calculated for C₂₅H₂₁O₂N₃F [M+H]⁺ 414.16123; found: 414.16093.

4.2.20 (Z)-3-((4-chlorophenyl)amino)-1-(3-(4-methoxyphenyl)-1-phenyl-1H-pyrazol-4-yl)prop-2-en-1-one (26)

Yellow solid, yield 78%, mp: 187-189 °C; ¹H NMR (300 MHz, CDCl₃) δ 11.88 (d, *J* = 12.1 Hz, 1H), 8.43 (s, 1H), 7.79 (d, *J* = 7.6 Hz, 2H), 7.74 – 7.69 (m, 2H), 7.50 (t, *J* = 7.9 Hz, 2H), 7.36 (d, *J* = 7.4 Hz, 2H), 7.32–7.26 (m, 4H), 7.00 (t, *J* = 8.6 Hz, 2H), 5.56 (d, *J* = 7.9 Hz, 1H), 3.88 (s, 3H). ¹³C NMR (75 MHz, CDCl₃) δ 186.5, 160.0, 152.5, 143.4, 143.1, 139.4, 139.0, 138.8, 130.7, 129.9, 129.7, 129.5, 128.3, 127.2, 125.3, 123.7, 119.4, 117.2, 117.1, 113.6, 97.3, 55.3. MS (ESI): 430 [M+H]⁺; 452 [M+Na]⁺; HRMS (ESI) calculated for C₂₅H₂₀O₂N₃ClNa [M+Na]⁺ 452.11363; found: 452.11365.

4.2.21 (Z)-1-(3-(4-methoxyphenyl)-1-phenyl-1H-pyrazol-4-yl)-3-((4-(trifluoromethyl)phenyl)amino)prop-2-en-1-one (27)

Brown solid, yield 67%, mp: 148-150 °C; ^1H NMR (300 MHz, CDCl_3) δ 11.93 (d, $J = 12.0$ Hz, 1H), 8.45 (s, 1H), 7.90 (d, $J = 8.8$ Hz, 2H), 7.86–7.68 (m, 4H), 7.54–7.41 (m, 2H), 7.11 (d, $J = 8.4$ Hz, 2H), 7.01 (t, $J = 8.9$ Hz, 2H), 6.81 (d, $J = 8.7$ Hz, 2H), 5.63 (d, $J = 7.9$ Hz, 1H), 3.89 (s, 3H). ^{13}C NMR (75 MHz, CDCl_3) δ 188.0, 169.3, 160.4, 160.1, 153.2, 152.7, 142.4, 138.9, 135.3, 130.7, 129.5, 127.9, 127.2, 127.0, 123.9, 122.3, 119.8, 119.4, 115.5, 113.6, 81.7, 55.4. MS (ESI): 464 $[\text{M}+\text{H}]^+$; HRMS (ESI) calculated for $\text{C}_{26}\text{H}_{21}\text{O}_2\text{N}_3\text{F}_3$ $[\text{M}+\text{H}]^+$ 411.1014; found: 464.15874.

4.2.22 (Z)-3-((4-hydroxyphenyl)amino)-1-(3-(4-methoxyphenyl)-1-phenyl-1H-pyrazol-4-yl)prop-2-en-1-one (28)

Brown solid, yield 79%, mp: 151-153 °C; ^1H NMR (300 MHz, CDCl_3) δ 11.88 (d, $J = 12.3$ Hz, 1H), 8.40 (s, 1H), 7.73 (dd, $J = 16.2, 8.2$ Hz, 4H), 7.47 (t, $J = 7.8$ Hz, 2H), 7.33 (t, $J = 7.4$ Hz, 1H), 7.20 (dd, $J = 12.0, 7.8$ Hz, 1H), 7.00 (d, $J = 8.7$ Hz, 2H), 6.90 (d, $J = 8.8$ Hz, 2H), 6.80 (d, $J = 8.8$ Hz, 2H), 5.46 (d, $J = 7.7$ Hz, 1H), 3.87 (s, 3H). ^{13}C NMR (75 MHz, CDCl_3) δ 186.0, 159.9, 152.9, 152.4, 145.4, 139.4, 133.3, 130.7, 129.9, 129.5, 127.1, 125.4, 123.8, 119.4, 118.0, 116.6, 113.7, 95.9, 55.3. MS (ESI): 412 $[\text{M}+\text{H}]^+$; 434 $[\text{M}+\text{Na}]^+$; HRMS (ESI) calculated for $\text{C}_{25}\text{H}_{21}\text{O}_3\text{N}_3\text{Na}$ $[\text{M}+\text{Na}]^+$ 434.14751; found: 434.14745.

4.2.23 (Z)-1-(3-(4-methoxyphenyl)-1-phenyl-1H-pyrazol-4-yl)-3-((4-methoxyphenyl)amino)prop-2-en-1-one (29)

Yellow solid, yield 82%, mp: 159-161 °C; ^1H NMR (300 MHz, CDCl_3) δ 11.93 (d, $J = 12.2$ Hz, 1H), 8.42 (s, 1H), 7.76 (dd, $J = 18.5, 8.0$ Hz, 4H), 7.50 (t, $J = 7.5$ Hz, 2H), 7.41 – 7.17 (m, 2H), 7.01 (d, $J = 7.1$ Hz, 4H), 6.89 (d, $J = 8.6$ Hz, 2H), 5.49 (d, $J = 7.6$ Hz, 1H), 3.89 (s, 3H), 3.81 (s, 3H). ^{13}C NMR (75 MHz, CDCl_3) δ 186.0, 160.0, 156.1, 152.3, 144.7, 139.4, 133.8, 130.6, 129.7, 129.5, 127.0, 125.5, 124.0, 119.3, 117.7, 114.9, 113.6, 96.0, 55.5, 55.3.

MS (ESI): 426 [M+H]⁺ and 448 [M+Na]⁺; HRMS (ESI) calculated for C₂₆H₂₄O₃N₃ [M +H]⁺ 426.18122; found: 426.18042

4.2.24 (Z)-1-(3-(4-methoxyphenyl)-1-phenyl-1H-pyrazol-4-yl)-3-((3,4,5-trimethoxyphenyl)amino)prop-2-en-1-one (30)

Yellow solid, yield 75%, mp: 148-150 °C; ¹H NMR (300 MHz, CDCl₃) δ 11.91 (d, *J* = 12.2 Hz, 1H), 8.42 (s, 1H), 7.78 (d, *J* = 7.9 Hz, 2H), 7.72 (d, *J* = 8.6 Hz, 2H), 7.49 (t, *J* = 7.8 Hz, 2H), 7.41 – 7.20 (m, 1H), 7.01 (d, *J* = 8.7 Hz, 2H), 6.83 (d, *J* = 8.6 Hz, 1H), 6.28 (s, 2H), 5.54 (d, *J* = 7.8 Hz, 1H), 3.88 (s, 3H), 3.86 (s, 6H), 3.81 (s, 3H). ¹³C NMR (75 MHz, CDCl₃) δ 186.2, 159.9, 154.1, 152.5, 144.0, 139.4, 136.5, 134.3, 130.7, 129.8, 129.5, 127.1, 125.4, 123.7, 119.4, 113.6, 96.5, 93.7, 61.0, 56.1, 55.3. MS (ESI): 486 [M+H]⁺; 508 [M+Na]⁺; HRMS (ESI) calculated for C₂₈H₂₇O₅N₃Na [M+Na]⁺ 508.18429; found: 508.18409.

4.2.25 (Z)-3-((4-fluorophenyl)amino)-1-(1-phenyl-3-(3,4,5-trimethoxyphenyl)-1H-pyrazol-4-yl)prop-2-en-1-one (31)

Pale yellow solid, yield 71%, mp: 169-171 °C; ¹H NMR (300 MHz, CDCl₃) δ 11.87 (d, *J* = 12.2 Hz, 1H), 8.36 (s, 1H), 7.71 (d, *J* = 7.8 Hz, 2H), 7.41 (t, *J* = 7.8 Hz, 2H), 7.27 (t, *J* = 7.3 Hz, 1H), 7.17 (d, *J* = 5.9 Hz, 1H), 7.15 (d, *J* = 4.4 Hz, 1H), 7.11 (s, 1H), 7.01 – 6.81 (m, 4H), 5.45 (d, *J* = 7.8 Hz, 1H), 3.83 (s, 9H). ¹³C NMR (75 MHz, CDCl₃) δ 186.1, 160.8, 157.6, 153.0, 152.4, 144.3, 139.3, 138.5, 136.6, 130.0, 129.5, 128.3, 127.3, 124.0, 119.4, 117.6, 116.6, 116.3, 106.9, 96.8, 61.0, 56.2. MS (ESI): 474 [M+H]⁺; HRMS (ESI) calculated for C₂₇H₂₅O₄N₃F [M+H]⁺ 474.18236; found: 474.18130.

4.2.26 (Z)-3-((4-chlorophenyl)amino)-1-(1-phenyl-3-(3,4,5-trimethoxyphenyl)-1H-pyrazol-4-yl)prop-2-en-1-one (32)

Pale yellow solid, yield 68%, mp: 185-187 °C; ¹H NMR (300 MHz, CDCl₃) δ 11.82 (d, *J* = 12.1 Hz, 1H), 8.33 (s, 1H), 7.68 (d, *J* = 7.8 Hz, 2H), 7.39 (t, *J* = 7.8 Hz, 2H), 7.25 (t, *J* = 7.4 Hz, 1H), 7.21 – 7.08 (m, 3H), 6.89 (s, 3H), 6.85 (s, 1H), 5.45 (d, *J* = 7.9 Hz, 1H), 3.80 (s, 9H). ¹³C NMR (75 MHz, CDCl₃) δ 186.4, 152.9, 152.5, 143.5, 139.3, 138.9, 138.5, 130.1, 129.7, 129.5, 128.5, 128.3, 127.3, 124.0, 119.4, 117.2, 106.8, 97.4, 60.9, 56.2. MS (ESI): 490 [M+H]⁺; HRMS (ESI) calculated for C₂₇H₂₅O₄N₃Cl [M+H]⁺ 490.15281; found: 490.15275.

4.2.27 (Z)-1-(1-phenyl-3-(3,4,5-trimethoxyphenyl)-1H-pyrazol-4-yl)-3-((4-(trifluoromethyl)phenyl)amino)prop-2-en-1-one (33)

Pale yellow solid, yield 79%, mp: 191-193 °C; ¹H NMR (500 MHz, CDCl₃) δ 11.97 (d, *J* = 12.0 Hz, 1H), 8.46 (s, 1H), 7.80 (dd, *J* = 10.4, 9.6 Hz, 2H), 7.57 (t, *J* = 9.1 Hz, 2H), 7.50 (t, *J* = 7.9 Hz, 2H), 7.37 (d, *J* = 7.4 Hz, 1H), 7.36 – 7.29 (m, 1H), 7.11 (d, *J* = 8.4 Hz, 2H), 6.99 (s, 2H), 5.62 (d, *J* = 8.0 Hz, 1H), 3.92 (s, 3H), 3.91 (s, 6H). ¹³C NMR (75 MHz, CDCl₃) δ 186.7, 153.1, 152.6, 143.1, 142.5, 139.2, 138.6, 130.2, 129.6, 128.1, 127.4, 127.1, 123.8, 119.5, 115.5, 106.8, 98.4, 60.9, 56.2. MS (ESI): 524 [M+H]⁺; HRMS (ESI) calculated for C₂₈H₂₅O₄N₃F₃ [M+H]⁺ 524.17917; found: 524.17888.

4.2.28 (Z)-3-((4-hydroxyphenyl)amino)-1-(1-phenyl-3-(3,4,5-trimethoxyphenyl)-1H-pyrazol-4-yl)prop-2-en-1-one (34)

White solid, yield 73%, mp: 171-173 °C; ¹H NMR (300 MHz, CDCl₃) δ 11.95 (d, *J* = 12.4 Hz, 1H), 8.45 (s, 1H), 7.78 (d, *J* = 7.7 Hz, 2H), 7.49 (t, *J* = 7.8 Hz, 2H), 7.36 (t, *J* = 7.4 Hz, 1H), 7.22 (dd, *J* = 9.0, 3.2 Hz, 1H), 7.00 (s, 2H), 6.92 (d, *J* = 8.8 Hz, 2H), 6.82 (d, *J* = 8.8 Hz, 2H), 5.48 (d, *J* = 7.7 Hz, 1H), 3.92 (s, 3H), 3.91 (s, 6H). ¹³C NMR (75 MHz, CDCl₃) δ 185.7, 152.9, 152.3, 145.3, 139.3, 138.4, 133.3, 130.0, 129.5, 128.4, 127.2, 124.1, 119.5, 118.0, 116.5, 106.8, 95.9, 60.9, 56.2. MS (ESI): 472 [M+H]⁺; HRMS (ESI) calculated for C₂₇H₂₆O₅N₃ [M+H]⁺ 472.18670; found: 472.18583.

4.2.29 (Z)-3-((4-methoxyphenyl)amino)-1-(1-phenyl-3-(3,4,5-trimethoxyphenyl)-1H-pyrazol-4-yl)prop-2-en-1-one (35)

White solid, yield 81%, mp: 178-180 °C; ¹H NMR (300 MHz, CDCl₃) δ 12.00 (d, *J* = 12.3 Hz, 1H), 8.45 (s, 1H), 7.80 (d, *J* = 7.9 Hz, 2H), 7.50 (t, *J* = 7.7 Hz, 2H), 7.36 (t, *J* = 7.3 Hz, 1H), 7.31 – 7.18 (m, 2H), 7.01 (d, *J* = 5.0 Hz, 2H), 6.89 (d, *J* = 8.8 Hz, 2H), 5.50 (d, *J* = 7.7 Hz, 1H), 3.90 (d, *J* = 16.7 Hz, 9H), 3.80 (s, 3H). ¹³C NMR (75 MHz, CDCl₃) δ 185.7, 156.3, 153.0, 152.3, 144.9, 139.42, 138.4, 133.8, 129.9, 129.5, 128.5, 127.2, 124.3, 119.4, 117.7, 115.0, 106.9, 96.1, 60.9, 56.2, 55.5. MS (ESI): 486 [M+H]⁺; HRMS (ESI) calculated for C₂₈H₂₈O₅N₃ [M+H]⁺ 486.20235; found: 486.20118.

4.2.30 (Z)-1-(1-phenyl-3-(3,4,5-trimethoxyphenyl)-1H-pyrazol-4-yl)-3-((3,4,5-trimethoxyphenyl)amino)prop-2-en-1-one (36)

White solid, yield 84%, mp: 169-171 °C; ¹H NMR (500 MHz, CDCl₃) δ 11.96 (d, *J* = 12.2 Hz, 1H), 8.45 (s, 1H), 7.79 (d, *J* = 7.9 Hz, 2H), 7.49 (dd, *J* = 17.0, 9.1 Hz, 2H), 7.35 (t, *J* = 7.2 Hz, 1H), 7.29 (t, *J* = 8.9 Hz, 1H), 6.98 (s, 2H), 6.28 (s, 2H), 5.52 (d, *J* = 7.8 Hz, 1H), 3.91 (s, 9H), 3.86 (s, 6H), 3.80 (s, 3H). ¹³C NMR (75 MHz, CDCl₃) δ 185.8, 158.7, 153.9, 151.9, 143.8, 139.7, 136.6, 134.4, 130.8, 129.7, 129.5, 127.1, 125.2, 123.7, 119.4, 113.5, 96.7, 93.2, 60.9, 56.3, 55.1. MS (ESI): 546 [M+H]⁺; HRMS (ESI) calculated for C₃₀H₃₂O₇N₃ [M+H]⁺ 546.22348; found: 546.22283.

4.3 Cell culture

HT-29 (colon), PC-3 (prostate), A549 (lung) and U87MG (brain) cancer cells were purchased from ATCC (Manassas, VA) and keratinocytes (HaCaT) were procured from Life Technologies. PC-3, A549 and HaCaT cells were grown in Roswell Park Memorial Institute (RPMI-1640) medium (GIBCO-Invitrogen, NY) with 10% fetal bovine serum (FBS)

supplemented with glutamine (2 mmol/L), penicillin G (100 µg/mL)/ streptomycin (100 µg/mL) at 37 °C under 5% CO₂. HT-29 and U87MG cells were grown in Dulbecco's modified Eagle's (DMEM) medium containing 10% FBS, 1% penicillin/ streptomycin at 37 °C under 5% CO₂. The growth medium was changed every two days. After reaching 80-90% confluency, cells were treated with 0.25% trypsin-EDTA for further passage.

4.3.1 MTT assay

HT-29, U87MG, A549, PC-3 and HaCaT cells were used to test the cytotoxicity of the synthesized pyrazolo-triazole compounds (**7-36**). The cells under study were collected with 0.25% trypsin-EDTA, counted and seeded into a 96 well plate at a density of 3,000-5,000 cells per well depending on their doubling times. The cells were allowed to grow for 24 h at 37 °C and 5% CO₂. The culture media was removed after 24 h incubation and treated with 100 µL of test compounds. Then, the cells were further incubated with the compounds for 48 h under the same conditions. The culture medium containing compounds was removed after 48 h and 100 µL of culture media containing 5 mg/mL MTT (Thiazoyl blue tetrazolium bromide) was added to each well and cells were incubated for 4 hours. After 4 h incubation, the media containing MTT was aspirated off and 100 µL DMSO was added to each well to solubilize the crystallized formazan product. The plates were then read on a microplate reader at 570 nm and at a reference wavelength of 630 nm. The absorbance readings for 630 nm were subtracted from the 570 nm readings and the results were adjusted by dividing the average by control to adjust for any toxicity that may have occurred in this control treatment set. The percentage inhibition was calculated as $100 - [(Mean\ OD\ of\ treated\ cell \times 100) / Mean\ OD\ of\ vehicle\ treated\ cells\ (DMSO)]$. The IC₅₀ Values were calculated using Probit Software. All the tests were repeated in at least three independent experiments, while each experiment was performed in quadruplets.

4.3.2 *In vitro* migration assay

The wound-healing assay is a proven method to study cell migration. A549 cells (5×10^5 cells/well) were grown in 6 well plates as confluent monolayers for 24 hours. Then the monolayers were scratched with 200 μ L pipette tip and washed twice with PBS to remove non-adherent cells. The media containing IC_{50} concentrations of the test compounds **16**, **22** and **28** were added to each well. Then, cells which migrated across the wound area were photographed under the phase contrast microscope (Nikon) immediately after scratch (0 h), and at 24 h and 48 time interval after treatment in three or more randomly selected fields.

4.3.3 F-actin staining

A549 cells (1×10^6 cells/well) were grown on coverslips in 6 well plates for 24 h and then incubated with the compounds **16**, **22** and **28** for 12 h. After the compound treatment, cells were washed with PBS and fixed with 4% *para*-formaldehyde in PBS. Cells were incubated with rhodamine phalloidin for actin staining and Hoechst 33242 for nucleus staining. After washing thrice with PBS, cells were mounted with ProLong Gold anti-fade reagent (Molecular Probes, Eugene, OR) on microscopic slide and were observed by confocal microscopy (Nikon). Images were captured using 20X objective lenses.

4.3.4 Cell cycle analysis

A549 cells (1×10^6 cells /well) in 6 well plate were treated with IC_{50} concentrations of the compounds **16**, **22** and **28** for 24 h. Cells were collected by trypsinisation, washed with 150 mM PBS and were fixed with 70 % ethanol for 30 min at 4 °C. After fixing, cells were washed with PBS and stained with 400 μ L of Propidium Iodide staining buffer [PI (200 μ g), Triton X (100 μ L), DNase-free RNase A (2 mg) in 10 mL PBS] for 15 min at room temp in

dark. The samples were then analyzed for propidium iodide fluorescence from 15,000 events by flow cytometry using BD Accuri C6 flow-cytometer.

4.3.5 Hoechst staining

The nuclear morphology of A549 cells after treatment with the compounds was analyzed using Hoechst 33242. Cells (1×10^6 cells/well) at their growth phase were grown on cover slips in 6 well plates and were incubated with IC_{50} concentrations of the compounds **16**, **22** and **28** for 24 h. After 24 h incubation, cells were washed with 150 mM PBS and fixed with 4% *para*-formaldehyde solution at 4 °C for 10 min. Then, cells were washed twice with PBS and stained with Hoechst 33242 (5 μ g/mL) for 20 min at room temp and again cells were washed twice with PBS to remove excess dye. Cells were examined for morphological changes under confocal microscope using 350 nm excitation and 460 nm emission (Nikon, magnification 20X).

4.3.6 Measurement of mitochondrial membrane potential ($D\Psi_m$)

Intracellular $D\Psi_m$ in A549 cells was investigated using mitochondria specific rhodamine 123 dye. In this assay, A549 cells were cultured in 6 well plates at a density of 5×10^5 cells/mL and allowed to adhere overnight. The cells were treated with the IC_{50} concentrations of the test compounds **16**, **22** and **28** for 24 h. After 24 h treatment, the cells were harvested by trypsinisation, washed with PBS and resuspended in solution of PBS containing rhodamine-123 (10 μ g/mL) and further incubated for 30 min at room temp. Cells were washed twice with PBS to remove excess dye and resuspended in PBS. The samples were analyzed for rhodamine fluorescence using spectrofluorometer with an excitation and emission wavelengths of 480 and 530 nm.

4.3.7 Measurement of intracellular reactive oxygen species (ROS) levels

For analysis of ROS, A549 cells (2×10^5 cells/well) were plated in 24 well plates and allowed to grow for 24 h for attachment and then further incubated with the IC_{50} concentrations of the compounds **16**, **22** and **28** for 24 h. After treatment with the compounds, cells were washed with PBS and fixed with 4% *para*-formaldehyde. After fixing, cells were washed with PBS and incubated with carboxy-DCFDA (10 μ M) and images were capture using fluorescence microscope with an excitation 485 nm and emission 535 nm.

Acknowledgements

T.S.R. and H.K. are thankful to IICT-RMIT Research Centre for the award of research fellowships towards their Ph.D. V.B. acknowledges the Australian Research Council (ARC) for a Future Fellowship (FT140101285). V.B. and R.S. acknowledge the ARC for research support through the ARC-Linkage (LP130100437) scheme. R.S. acknowledges the support of Maxwell Eagle Endowment for cancer research. V.B. acknowledges the Ian Potter Foundation for supporting the establishment of the Ian Potter NanoBioSensing Facility at RMIT University and providing equipment support through various funding mechanisms.

References

1. R. Seigel, D. Naishadham, A. Jemal, Cancer statistics, 2013, CA Cancer J. Clin. 63 (2013) 11-30.
2. G. Kibria, H. Hatakeyama, H. Harashima, Cancer multidrug resistance: mechanisms involved and strategies for circumvention using a drug delivery system, Arch. Pharm. Res. 37 (2014) 4-15.
3. S.H. Kaufmann, W.C. Earnshaw, Induction of apoptosis by cancer chemotherapy, Exp. Cell Res. 256 (2000) 42-49.
4. R.J. Bold, P.M. Termuhlen, D.J. McConkey, Apoptosis, cancer and cancer therapy Surg. Oncol. 6 (1997) 133-142.
5. S.W. Fesik, Promoting apoptosis as a strategy for cancer drug discovery, Nat. Rev. Cancer 5 (2005) 876-885.
6. V. Kumar, K. Kaur, G.K. Gupta, A.K. Sharma, Pyrazole containing natural products: synthetic preview and biological significance, Eur. J. Med. Chem. 69 (2013) 735-753.
7. V. Kumar, R. Aggarwal, P. Tyagi, Synthesis and antibacterial activity of some new 1-heteroaryl-5-mino-4-phenyl-3-trifluoromethylpyrazoles, Eur. J. Med. Chem. 40 (2005) 922-927.
8. R. Gondru, J. Banothu, R.K. Thatipamula, S.K. Althaf Hussain, R. Bavantula, 3-(1-Phenyl-4-((2-(4-arylthiazol-2-yl) hydrazono) methyl)-1H-pyrazol-3-yl)-2H-chromen-2-ones: one-pot three component condensation, *in vitro* antimicrobial, antioxidant and molecular docking studies, RSC Adv. 5 (2015) 33562-33569.
9. J.B. Shi, W.J. Tang, R. Li, X.H. Liu, Novel pyrazole-5-carboxamide and pyrazole-pyrimidine derivatives: Synthesis and anticancer activity, Eur. J. Med. Chem. 90 (2015) 889-896.

10. H. Kumar, D. Saini, S. Jain, N. Jain, Pyrazole scaffold: A remarkable tool in the development of anticancer agents, *Eur. J. Med. Chem.* 70 (2013) 248-258.
11. A.Kamal, A.B. Shaik, N. Jain, C. Kishor, A. Nagabhushana, B. Supriya, G.B. Kumar, S.S. Chourasiya, Y. Suresh, R.K. Mishra, A. Addlagatta, Design and synthesis of pyrazole–oxindole conjugates targeting tubulin polymerization as new anticancer agents, *Eur. J. Med. Chem.* 92 (2015) 501-513.
12. F.K. Keter, J. Darkwa, Perspective: the potential of pyrazole-based compounds in medicine, *Biometals* 25 (2012) 9-21.
13. Y. Luo, Y. Zhou, J. Fu, H.L. Zhu, 4, 5-Dihydropyrazole derivatives containing oxygen-bearing heterocycles as potential telomerase inhibitors with anticancer activity, *RSC Adv.* 4 (2014) 23904-23913.
14. Y. Xia, C.D. Fan, B.X. Zhao, J. Zhao, D.S. Shin, J.Y. Miao, Synthesis and structure–activity relationships of novel 1-arylmethyl-3-aryl-1*H*-pyrazole-5-carbohydrazone derivatives as potential agents against A549 lung cancer cells, *Eur. J. Med. Chem.* 43 (2008) 2347–2353.
15. A. Kamal, G.B. Kumar, S. Polepalli, A.B. Shaik, V.S. Reddy, M.K. Reddy, Ch.R. Reddy, R. Mahesh, J.S. Kapure, N. Jain, Design and Synthesis of Aminostilbene–Arylpropenones as Tubulin Polymerization Inhibitors, *ChemMedChem* 9 (2014) 2565-2579.
16. A. Kamal, V.S. Reddy, A.B. Shaik, G.B. Kumar, M.V. Vishnuvardhan, S. Polepalli, N. Jain, Synthesis of (*Z*)-(arylamino)-pyrazolyl/isoxazolyl-2-propenones as tubulin targeting anticancer agents and apoptotic inducers, *Org. Biomol. Chem.* 13 (2015) 3416–3431.
17. M.V. Reddy, B. Akula, S.C. Cosenza, C.M. Lee, M.R. Mallireddigari, V.R. Pallela, D.R. Subbaiah, A. Udofa, E.P. Reddy, (*Z*)-1-Aryl-3-arylamino-2-propen-1-ones, highly active stimulators of tubulin polymerization: synthesis, structure–activity relationship (SAR),

- tubulin polymerization, and cell growth inhibition studies, *J. Med. Chem.* 55 (2012) 5174-5187.
18. T.S. Reddy, H. Kulhari, V.G. Reddy, A.S. Rao, V. Bansal, A. Kamal, R. Shukla, Synthesis and biological evaluation of pyrazolo–triazole hybrids as cytotoxic and apoptosis inducing agents, *Org. Biomol. Chem.* 13 (2015) 10136-10149.
 19. T.S. Reddy, H. Kulhari, V.G. Reddy, V. Bansal, A. Kamal, R. Shukla, Design, synthesis and biological evaluation of 1,3-diphenyl-1*H*-pyrazole derivatives containing benzimidazole skeleton as potential anticancer and apoptosis inducing agents, *Eur. J. Med. Chem.* 101 (2015) 790-805.
 20. T. Mosmann, Rapid colorimetric assay for cellular growth and survival: Application to proliferation and cytotoxicity assays, *J. Immunol. Meth.* 65 (1983) 55–63.
 21. L.G. Rodriguez, X. Wu, J. L. Guan, Wound healing assay, *Methods Mol. Biol.* 294 (2005) 23–29.
 22. C.L. Clainche, M.F. Carlier, Regulation of actin assembly associated with protrusion and adhesion in cell migration, *Physiol. Rev.* 88 (2008) 489–513.
 23. D. Vignjevic, G. Montagnac, Reorganization of the dendritic actin network during cancer cell migration and invasion, *Semin. Cancer Biol.* 18 (2008) 12-22.
 24. Y. Zhao, W. Liu, Y. Zhou, X. Zhang, P.V. Murphy, *N*-(8-(3-ethynylphenoxy) octyl)-1-deoxyojirimycin suppresses growth and migration of human lung cancer cells, *Bioorg. Med. Chem. Lett.* 20 (2010) 7540-7543.
 25. A. Kamal, P. Suresh, M.J. Ramaiah, T. Srinivasareddy, R.K. Kapavarapu, B.N. Rao, S. Imthiajali, T. Lakshminarayanreddy, S.N.C.V.L. Pushpavalli, N. Shankaraiah, M. Pal-Bhadra, 4β-[4'-(1-(Aryl) ureido) benzamide] podophyllotoxins as DNA topoisomerase I and IIα inhibitors and apoptosis inducing agents, *Bioorg. Med. Chem.* 21 (2013) 5198-5208.

26. W. Xia, S. Spector, L. Hardy, S. Zhao, A. Saluk, L. Alemane, N.L. Spector, Tumor selective G2/M cell cycle arrest and apoptosis of epithelial and hematological malignancies by BBL22, a benzazepine, *Proc. Natl. Acad. Sci. USA*, 97 (2000) 7494–7499.
27. G. Ouyang, L. Yao, K. Ruan, G. Song, Y. Mao, S. Bao, Genistein induces G2/M cell cycle arrest and apoptosis of human ovarian cancer cells via activation of DNA damage checkpoint pathways, *Cell Biology International*, 33 (2009) 1237–1244.
28. S. Schwarz, B. Siewert, R. Csuk, A.P. Rauter, New antitumor 6-chloropurine nucleosides inducing apoptosis and G2/M cell cycle arrest, *Euro. J. Med. Chem.* 90 (2015) 595-602.
29. S. Allen, J. Sotos, M.J. Sylte, C.J. Czuprynski, Use of Hoechst 33342 staining to detect apoptotic changes in bovine mononuclear phagocytes infected with *Mycobacterium avium* subsp. *Paratuberculosis*, *Clin. Diagn. Lab Immunol.* 8 (2001) 460–464.
30. J.D. Ly, D.R. Grubb, A. Lawen, The mitochondrial membrane potential ($\Delta\psi(m)$) in apoptosis; an update, *Apoptosis* 8 (2003) 115–128.
31. R.K. Emasus, R. Grunwald, J.J. Lemasters, Rhodamine 123 as a probe of transmembrane potential in isolated rat-liver mitochondria: spectral and metabolic properties, *Biochim. Biophys. Acta* 850 (1986) 436–448.
32. N. Zamzami, P. Marchetti, M. Castedo, D. Decaudin, A. Macho, T. Hirsch, S.A. Susin, P.X. Petit, B. Mignotte, G. Kroemer, Sequential reduction of mitochondrial trans membrane potential and generation of reactive oxygen species in early programmed cell death, *J. Exp. Med.* 182 (1995) 367–377.

Figure/Scheme Captions

Scheme 1. General synthesis of (*Z*)-1-(1,3-diphenyl-1*H*-pyrazol-4-yl)-3-(phenylamino)prop-2-en-1-one (**7-36**). Reagents and conditions: (a) ethanol, 50–60 °C, 3 h; (b) DMF, POCl₃, 50–60 °C, 5 h; (c) ethynylmagnesium bromide, THF, 0 °C, RT, 8-9 h, 60-70%; (d) 2-iodoxybenzoic acid, DMSO, RT, 5 h, 70-72%; (e) different substituted anilines, ethanol, 80 °C, 3 h.

Table 1. *In vitro* anti-proliferative activity (IC₅₀ - μM) of compounds (**7-36**).

Figure 1. Effect of compounds **16**, **22** and **28** on migration of A549 lung cancer cells. The images were captured using phase contrast microscopy before (0 h), and after 24 and 48 h of treatment with the compounds.

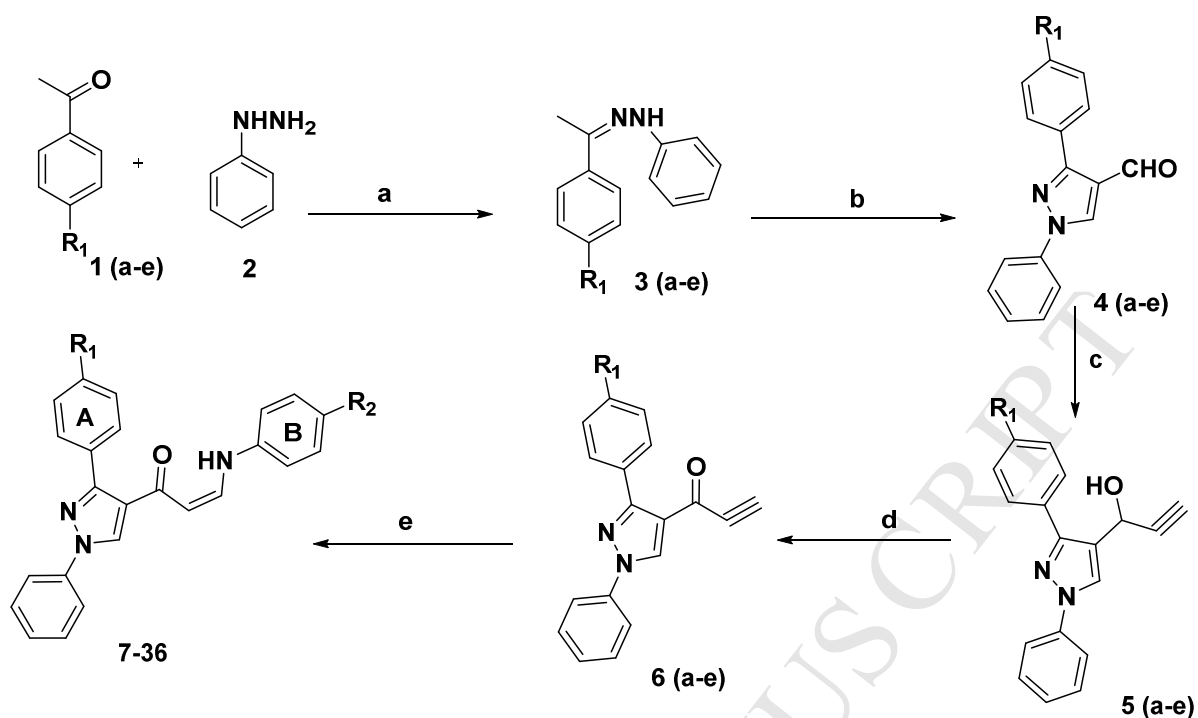
Figure 2. Effect of compounds **16**, **22** and **28** on actin stress fibre polymerisation in A549 lung cancer cells, as assessed by fluorescence staining with Hoechst 33242 (nucleus: blue) and rhodamine-phalloidin (actin filaments: red). Control A549 cells display intact stress fibres (green arrow), whereas compounds treatments lead to marked disruption of stress fibre assembly.

Figure 3. Effect of compounds **16**, **22** and **28** on cell cycle arrest of A549 lung cancer cells, as determined by flow-cytometry using propidium iodide staining (left panel). The percentage of cells in each phase was quantified using BD Accuri C6 software (right panel). Data are mean ± standard deviation from three independent experiments.

Figure 4. Effect of compounds **16**, **22** and **28** on nuclear morphological changes of A549 cells. Cells were treated with IC₅₀ concentrations of compounds for 24 h and stained with Hoechst 33242. Fragmented nuclei and apoptotic bodies are indicated by arrows.

Figure 5. Effect of compounds **16**, **22** and **28** on mitochondrial membrane potential ($\Delta\Psi_m$). A549 cells were treated with compounds **16**, **22** and **28** for 24 h and incubated with Rhodamine 123. The intensity of Rhodamine 123 fluorescence was determined by fluorescence spectrophotometer. Data are mean \pm standard deviation from three independent experiments, each with triplicates.

Figure 6. Effect of compounds **16**, **22** and **28** on intracellular reactive oxygen species (ROS) levels. A549 cells treated with compounds **16**, **22** and **28** for 24 h and incubated with carboxy-DCFDA. The images (left panel) were captured with fluorescence microscopy and quantitative estimation of ROS (right panel) was determined using fluorescence spectrophotometer at an excitation wavelength of 485 nm and an emission wavelength of 535 nm.



Scheme 1. General synthesis of (*Z*)-1-(1,3-diphenyl-1*H*-pyrazol-4-yl)-3-(phenylamino)prop-2-en-1-one (**7-36**). Reagents and conditions: (a) ethanol, 50–60 °C, 3 h; (b) DMF, POCl₃, 50–60 °C, 5 h; (c) ethynylmagnesium bromide, THF, 0 °C, RT, 8-9 h, 60-70%; (d) 2-iodoxybenzoic acid, DMSO, RT, 5 h, 70-72%; (e) different substituted anilines, ethanol, 80 °C, 3 h.

Table 1. *In vitro* anti-proliferative activity (^aIC₅₀ - μM) of compounds (7-36).

Compound	R ₁	R ₂	HT29 ^b	PC3 ^c	A549 ^d	U87MG ^e	HaCaT ^f
7	H	F	6.87±0.89	7.98±0.57	4.67±1.3	10.23±2.6	34.2±3.5
8	H	Cl	3.61±0.56	5.2±0.93	14.05±0.76	11.4±0.29	28.4±4.1
9	H	CF ₃	>50	>50	>50	>50	>50
10	H	OH	5.0±0.96	3.6±0.65	3.21±1.2	4.29±0.89	44.6±3.6
11	H	OMe	1.56±0.32	6.4±1.1	3.25±0.19	>50	>50
12	H	3,4,5-OMe	9.8±1.3	5.93±1.7	6.34±0.83	2.35±0.65	36.2±1.8
13	F	F	6.5±0.62	7.9±1.34	5.78±0.13	18.2±3.6	>50
14	F	Cl	4.6±0.61	3.8±0.56	6.7±0.85	8.9±1.3	21.3±2.1
15	F	CF ₃	>50	>50	>50	>50	>50
16	F	OH	1.9±0.21	2.6±0.19	1.5±0.45	4.7±0.8	16.3±1.2
17	F	OMe	3.2±0.9	4.6±0.7	8.9±0.51	2.5±0.61	19.6±0.93
18	F	3,4,5-OMe	7.77±0.96	4.89±1.35	9.35±1.8	12.6±2.1	32.8±3.4
19	Cl	F	>50	>50	>50	17.85±3.56	>50
20	Cl	Cl	4.65±0.63	3.89±0.79	3.67±0.3	13.12±1.2	23.4±3.7
21	Cl	CF ₃	>50	>50	>50	>50	>50
22	Cl	OH	2.5±0.27	4.43±1.3	1.91±0.21	1.50±0.43	22.6±2.3
23	Cl	OMe	8.93±1.4	10.65±1.1	6.46±2.7	6.89±1.95	30.8±2.9
24	Cl	3,4,5-OMe	12.7±2.6	9.98±0.69	5.64±0.56	17.8±3.6	46.6±5.2
25	OMe	F	7.65±0.86	5.73±0.39	3.98±0.41	8.91±1.23	8.91±1.23
26	OMe	Cl	4.76±0.57	3.89±0.33	2.97±0.26	8.86±0.3	20.9±1.5
27	OMe	CF ₃	9.87±0.31	>50	>50	>50	>50
28	OMe	OH	2.46±0.57	1.98±0.16	2.77±0.24	3.73±0.66	34.6±2.5
29	OMe	OMe	8.76±0.98	13.4±1.7	6.78±3.4	>50	>50
30	OMe	3,4,5-OMe	14.6±1.7	18.9±2.3	11.2±1.65	>50	>50
31	3,4,5-OMe	F	12.5±1.21	7.7±0.67	15.6±0.96	4.78±0.54	25.7±1.3
32	3,4,5-OMe	Cl	7.68±0.92	11.2±1.43	8.67±0.75	3.21±0.36	30.2±2.8
33	3,4,5-OMe	CF ₃	>50	>50	>50	>50	>50
34	3,4,5-OMe	OH	2.5±0.09	4.6±0.78	3.16±0.92	1.8±0.57	17.6±1.1
35	3,4,5-OMe	OMe	5.78±1.9	9.6±1.7	4.78±0.41	12.8±2.3	>50
36	3,4,5-OMe	3,4,5-OMe	8.4±2.63	14.1±1.94	7.98±1.78	5.1±0.93	20.9±1.5
5-Fluorouracil			2.8±0.63	2.76±0.38	3.98±0.9	3.65±0.55	16.15±1.9

^aIC₅₀ values are the concentrations that cause 50% inhibition of cancer cell growth (μM). Data represent the mean values ± standard deviation of three independent experiments performed in triplicate, each with quadruplet; ^bcolon cell line; ^cprostate cancer cell line; ^dlung cancer cell line; ^eglioblastoma cell line; ^fhuman keratinocytes;

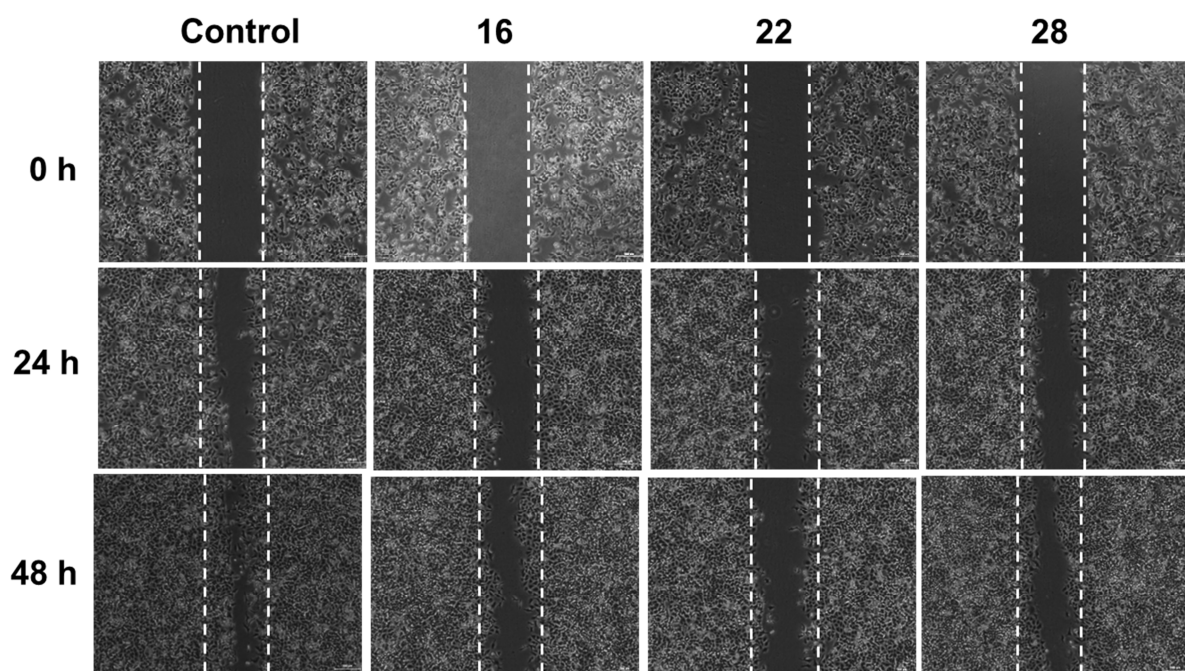


Figure 1. Effect of compounds **16**, **22** and **28** on migration of A549 lung cancer cells. The images were captured using phase contrast microscopy before (0 h), and after 24 and 48 h of treatment with the compounds..

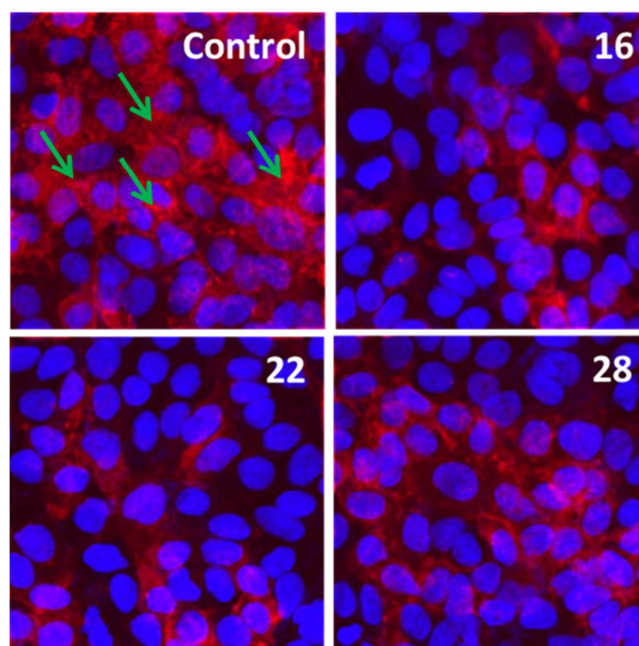


Figure 2. Effect of compounds **16**, **22** and **28** on actin stress fibre polymerisation in A549 lung cancer cells, as assessed by fluorescence staining with Hoechst 33242 (nucleus: blue) and rhodamine-phalloidin (actin filaments: red). Control A549 cells display intact stress fibres (green arrow), whereas compounds treatments lead to marked disruption of stress fibre assembly.

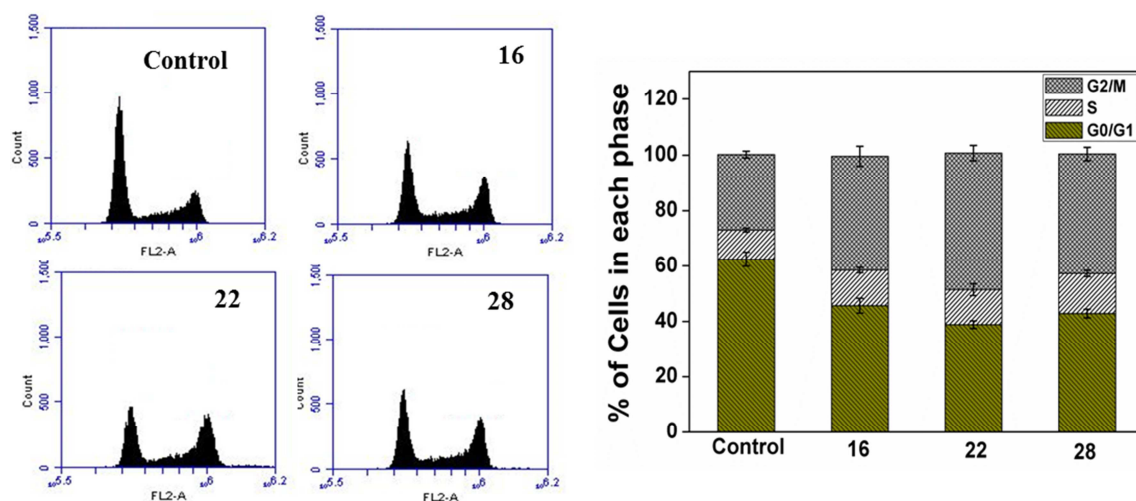


Figure 3. Effect of compounds **16**, **22** and **28** on cell cycle arrest of A549 lung cancer cells, as determined by flow-cytometry using propidium iodide staining (left panel). The percentage of cells in each phase was quantified using BD Accuri C6 software (right panel). Data are mean \pm standard deviation from three independent experiments.

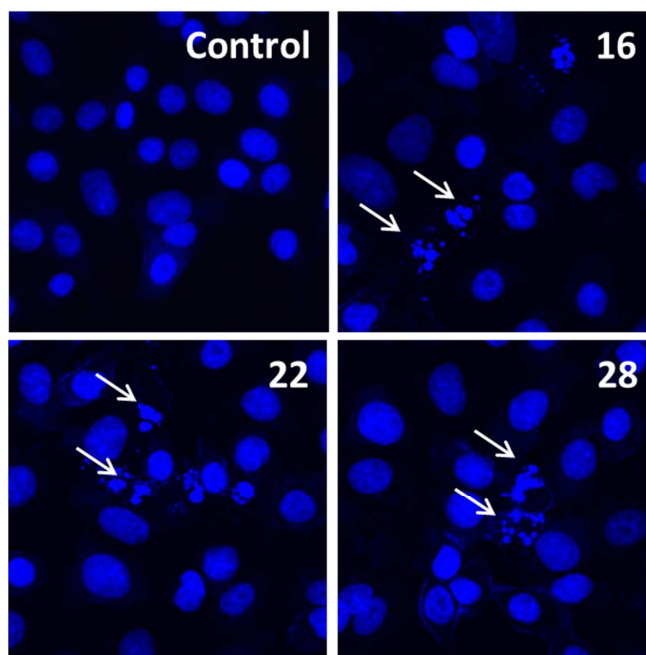


Figure 4. Effect of compounds **16**, **22** and **28** on nuclear morphological changes of A549 cells. Cells were treated with IC_{50} concentrations of compounds for 24 h and stained with Hoechst 33242. Fragmented nuclei and apoptotic bodies are indicated by arrows.

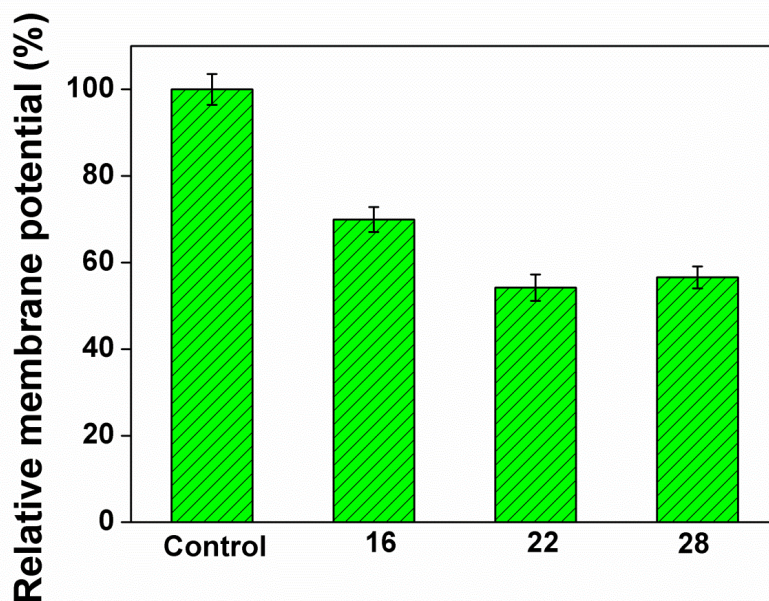


Figure 5. Effect of compounds **16**, **22** and **28** on mitochondrial membrane potential ($\Delta\Psi_m$). A549 cells were treated with compounds **16**, **22** and **28** for 24 h and incubated with Rhodamine 123. The intensity of Rhodamine 123 fluorescence was determined by fluorescence spectrophotometer. Data are mean \pm standard deviation from three independent experiments, each with triplicates.

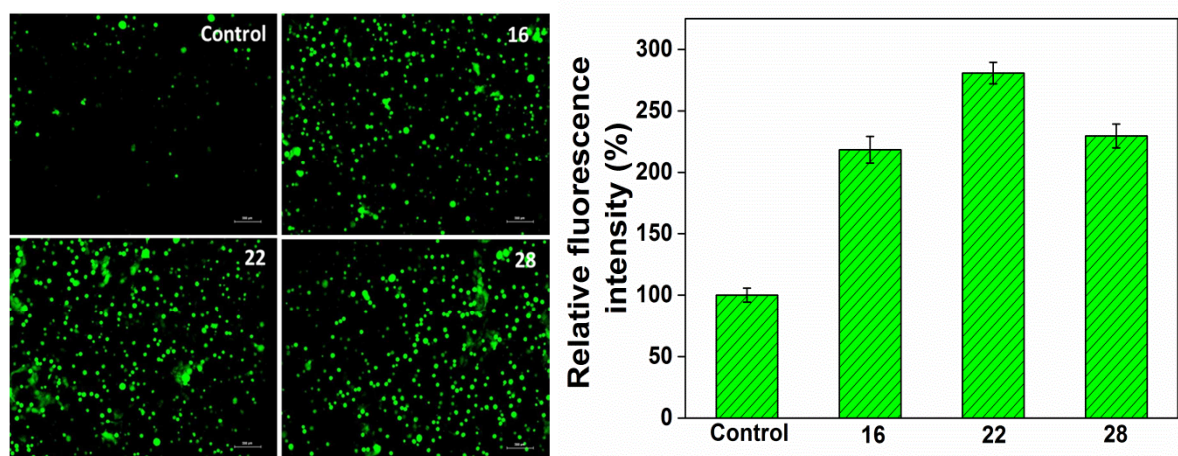


Figure 6. Effect of compounds **16**, **22** and **28** on intracellular reactive oxygen species (ROS) levels. A549 cells treated with compounds **16**, **22** and **28** for 24 h and incubated with carboxy-DCFDA. The images (left panel) were captured with fluorescence microscopy and quantitative estimation of ROS (right panel) was determined using fluorescence spectrophotometer at an excitation wavelength of 485 nm and an emission wavelength of 535 nm.

- A series of thirty (*Z*)-1-(1,3-diphenyl-1*H*-pyrazol-4-yl)-3-(phenylamino)prop-2-en-1-one derivatives were synthesized
- Most of the compounds were selectively cytotoxic against A549 lung cancer cells
- Three compounds **16**, **22** and **28** displayed promising anticancer activity
- These active compounds induced G2/M cell cycle arrest and apoptosis in A549 cells

ACCEPTED MANUSCRIPT